Estimation of the Primary Batteries State of Charge and State of Art by Frequency Characteristics of Electrochemical Impedance Spectra

Riabokin O.L., Bojchuk O.V., Pershina K.D.

Joint Department of Electrochemical Energy Systems NAS of Ukraine, Kiev, Vernadsky ave. 38-A, 03142

Electrochemical Impedance Spectroscopy (EIS) is widely used for measurement and study of the electrode materials and electrochemical properties of electrochemical devices [1-5]. There are many methods for obtaining various electrochemical parameters using EIS [1-5]. Moreover, the intercalation of ions into battery electrodes could be fixed by EIS spectra using their ability to response the solid-state transport of charge carriers in the active material at low frequencies [6]. It is well known that the transport of charge carriers is limited by ionic diffusion in many battery materials due to the high mobility of electrons [7, 8]. Traditionally the diffusion in battery electrodes with large particle sizes is described by Warburg-type diffusion impedance, which draws a 45° line in the complex plane representation (Nyquist plot), and is widely reported at low frequencies. Such response is well described by a linearized diffusion model [9]. But in primary batteries the electrode process consumes zincate ions and produces hydroxyl ions during charge in the zinc electrode compartment; inversely, during discharge it produces zincate ions and consumes hydroxyl ions [10]. In this case the transport of zinc material leads to a reduction of capacity and service life of a battery due to formation of zinc species which entrain zinc, such as Zn, ZnO, $Zn(OH)_2$, $K_2Zn(OH)_4$, $Zn(OH)_4^{2-}$ or polymeric zinc species, and decreases the size of particles on the electrode/electrolyte boundary [11]. Such processes lead to a significant deviation from linearity and can't be described by the linearized diffusion model, because the penetration depth of diffusion can reach the impermeable current collector of a thin electrode film or the

reflective center of a nanoparticle at accessible low frequencies, due to short diffusion lengths in the thin film and nanoparticles [7, 12 - 14]. Therefore, it's the reason to apply parameters that describe the nonlinear behavior of diffusion, in particular, the model of anomalous diffusion. This model gives relatively simple equations in the frequency domain based on frequency dependence of the differential capacitance from capacitance fractional derivatives and estimates the intensity of the ions motion, depending on the frequency change [15]. So, the purpose of the work is to apply the required frequency dependent parameters of the EIS to estimate the primary batteries state of charge and state of art.

1. Experimental

Alkaline zinc manganese primary batteries (Duracell) in AAA gross geometry (MN 2400) with a voltage of 1.5 V were chosen as the samples of test. The discharge of this batteries was carried out at the potentiostat in galvanostatic mode under DC - 10, 20, 30, 40, 50, 60 mA/cm^2 at a temperature of $(20 \pm 5)°C$ within 80 minutes in accordance to international standards [16]. Before the discharging, the samples were stood at 1.5 ± 0.2 h. for obtaining the temperature equilibrium in the electrochemical system. The value of discharge currents based on the nominal capacity of the batteries in A•h was calculated. Internal resistance at constant current was calculated by the formula:

$$R = \frac{U_i - U_f}{I_2 - I_1} \qquad (1)$$

$I_2 = 0{,}2 \cdot I_1$, I_1 - discharge currents.

The EIS spectra were recorded using an Autolab-30 electrochemical module (Ekochemie BV, Netherlands) equipped with a Frequency Response Analyzer module. The measurements were performed according to a standard procedure in the frequency range of 0.01 Hz to 1.0 MHz with a single pulse amplitude of ±5 mV into two electrode cell. The module was controlled using Autolab 4.7 software with the subsequent processing using the Zview 2.0 software package via the complex amplitude method.

2. Results and discussion

Impedance spectra of samples after various current external loads have established

a significant difference of their form (Fig. 1a, 2a). The typical displacements in the middle-frequency (10^2 - 10^3 Hz) and the low-frequency (10^{-1}-10^1 Hz) regions of the spectrum have been fixed too (Fig. 1b, 2b). So the Warburg-type diffusion impedance, which draws a 45∘ line in the complex plane representation, which has been widely reported at low frequencies, can't be applied, because in all the cases the line in the complex plane representation is below 45°. Such dependencies have been well described by anomalous diffusion model under the conditions of the adsorption limitation on the electrode/electrolyte interface [15]. In compliance with the model it is able to partition of the diffusion flows into two parts: the diffusion between the macro grains of the electrode materials:

$$J = -D \frac{\partial^{1-\gamma}}{\partial t^{1-\gamma}} \frac{\partial c}{\partial x} \qquad (2)$$

and diffusion between the microparticles:

$$\frac{\partial^{2-\gamma} C}{\partial t^{2-\gamma}} = D \frac{\partial^2 C}{\partial x^2} \qquad (3)$$

The first type of diffusion could be described by Fick's second law because in most active materials the mobility of electrons is much higher than that of ions. As electrons become freely available in the system, the mean electric field quickly relaxes, resulting in local charge neutrality in the bulk. Under such conditions ionic diffusion limits transport of the charge carriers, and a neutral diffusion equation, Fick's law, can be recovered for the ion material balance in the system. In this case the electrochemical double layer develops at the interface due to the potential drop across it. The double layer charging process can be modeled with the ideal capacitor equation [7]. Taking into account the potential drop of the dense part of the DL the capacitance is described by the equation:

$$C = {}^q/_{c_1} + {}^q/_{c_2} + {}^q/_{c_3} \qquad (4)$$

c_1, c_2, c_3 – differential capacitance of the various parts of DL

Thus the macroscopic capacitance can be calculated as:

$$C_{max} = 3R_{max}\omega_{max} \qquad (5)$$

Microscopic capacity corresponding to the degree of destruction of the electrode can be calculated by macroscopic capacitance fractional derivative:

$$C_{min} = \frac{1}{3R_{max}\omega_{max}^{2-\gamma}} \qquad (6)$$

So, it can get a visual picture of the battery electrode/electrolyte interface changes using a three-dimensional coordinate system (frequency, differential capacitance and capacitance fractional derivatives). The performance of the graphical integration demonstrates significant differences in the structure of electrode/electrolyte interface under different current loads (Fig. 1a, b, c, d), i.e. battery state of art. Such behavior of the batteries made it possible to assume the state of charge by simple calculation using the maximum shift of phase angle values and values of frequencies near this maximum (Fig. 1b, 2b).

$$f_r(t) = \frac{f_0}{\sqrt{1-\frac{t}{T_D}}} \qquad (7)$$

f_0 - the frequency of the maximum shift of phase angle of the charged element, t - time, T_D - time of shift when discharged [2]. Then, taking into account the shift of the frequency range of the:

$$SOC = \frac{f_{TD}}{f_0} \times 100\% \qquad (8)$$

Also, the linear dependence has the ratio of absolute values of the phase angle shift:

$$SOC = \frac{\theta_{TD}}{\theta_0} \times 100\% \qquad (9)$$

Batteries state of charge calculations by different methods (Table 1) show constitutive differences in charge values and mistakes of measurements, especially under high current density. Using of eq. 7 significantly increased batteries SOC values. This allows us to suppose that this method of calculation is incorrect. The SOC calculation by maximum phase angle shift gave more correct results. That allowed us to offer it as an express test of the battery SOC.
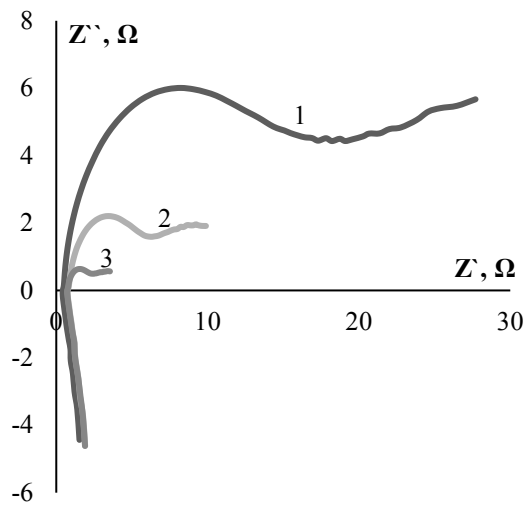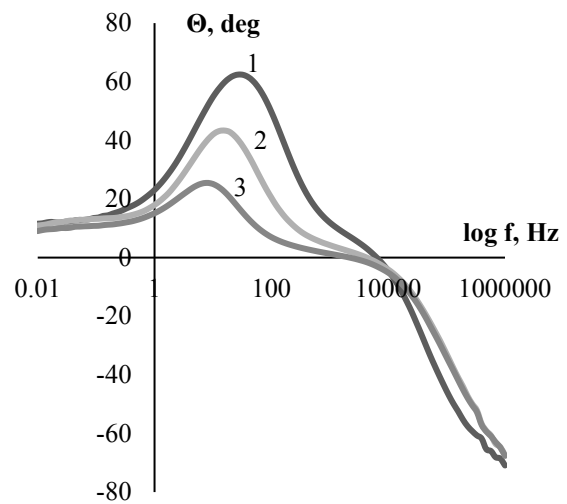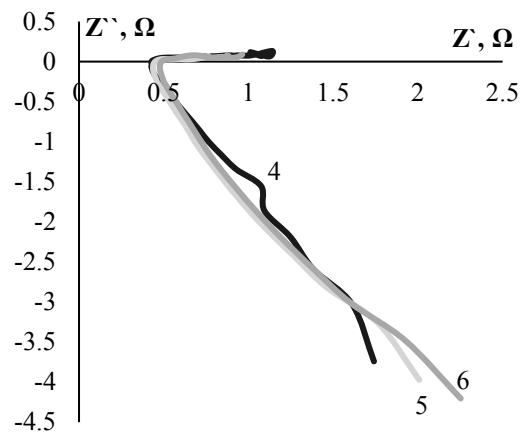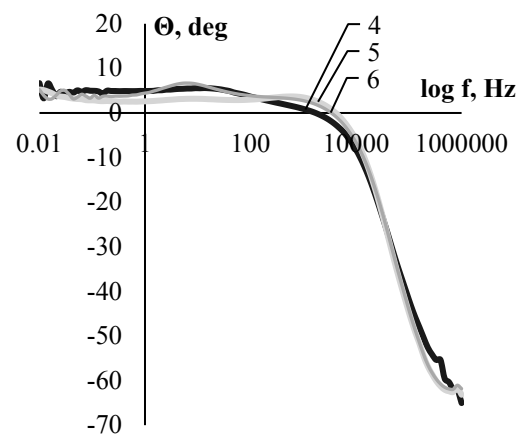
Fig. 1. EIS of batteries after discharge in Nyquist coordinates (a) 1 - 10 mA/cm^2, 2 - 20 mA/cm^2, 3 - 30 mA/cm2; (c) 4 - 40 mA/cm^2, 5 - 50 mA/cm^2, 6 - 60 mA/cm^2. In Bode coordinates after discharge: (b) 1 - 10 mA/cm^2; 2 - 20 mA/cm^2, 3 - 30 mA/cm2, (d) 4 - 40 mA/cm^2, 5 - 50 mA/cm^2, 6 - 60 mA/cm^2
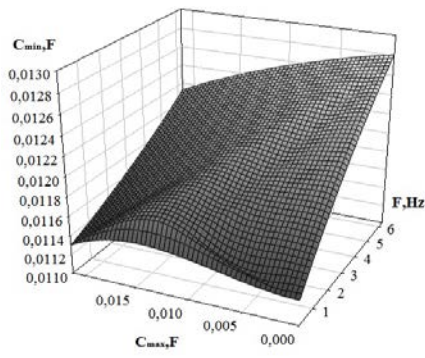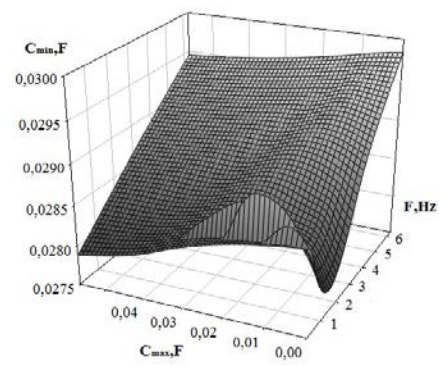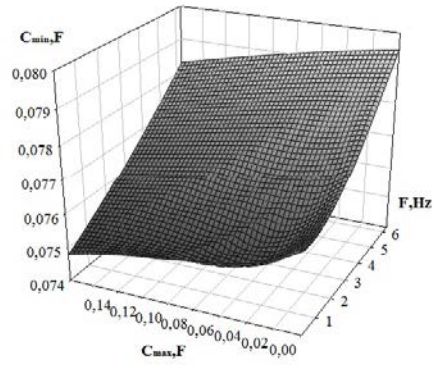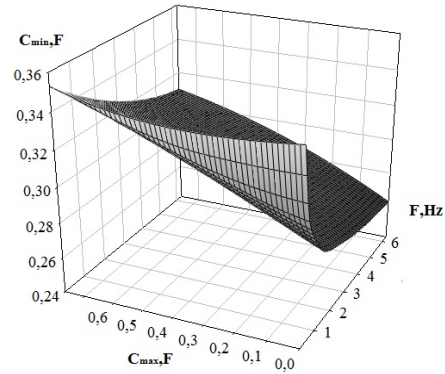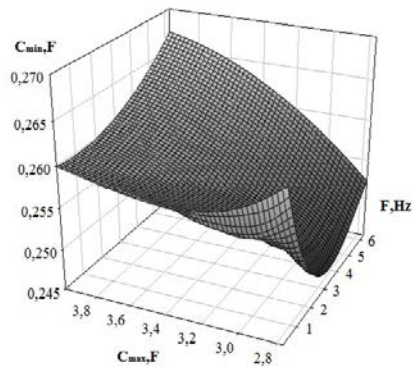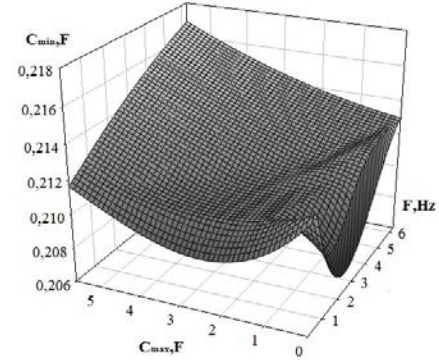
Fig. 2. 3D discharge diagram at (a) 10 mA / cm^2, (b) 2 - 20 mA/cm^2, (c) 3 - 30 mA/cm2, (d) 4 - 40 mA/cm^2, (e) 5 - 50 mA/cm^2, (f) 6 - 60 mA/cm^2 in the low frequency range

Table 1. Results of battery charge measurements by different methods

Density of discharge current, mA/cm^2	Maximum of initial frequency f_0, Hz	Maximum of frequency after discharging f_{TD}, Hz	The value of the phase angle shift Θ, deg	Calculated SOC by eq.7 , %	Calculated SOC by eq.9, %	SOC according to standard measurements, %
0	57,50	57,50	76,22	0	0	0
10	57,50	33,11	62,33	42±2,7	18±0,5	12±1,5
20	57,50	19,05	42,94	67±2,4	44±0,5	44±1.5
30	57,50	10,97	24,76	81±7,6	68±0,5	68±1,5
40	57,50	10,97	5,50	89±9,5	93±0,7	60±5,5
50	57,50	10,97	3,17	89±10,5	96±0,7	52±10,4

3. Conclusion

The application of the frequency dependent EIS parameters in low frequency range estimates the primary batteries state of charge and state of art. Data application of three-dimensional coordinate system (frequency,   differential capacitance and fractional derivatives from this capacitance) makes it possible to perform a graphical integration procedure. This procedure demonstrates significant differences in the structure of electrode/electrolyte interface under different current loads, and gives an opportunity for battery state of art estimation. The state of batteries charge estimated by different methods has shown constitutive differences in charge values, especially under high current density. Method based on the ratio of frequencies near maximum shift of phase angle has the highest deviation relative to the standard method of the battery SOC estimation. The SOC calculation by maximum phase angle shift has given more correct results and minimal mistakes during measurements. The ratio of maximum phase angle shift has been proposed as express test of the battery SOC.

References

[1] J.P. Christophersen, C.G. Motloch, J.L. Morrison, W. Albrecht, , U.S. Patent, No. US 2007/0257681 (2007).

[2] H.J. Daniel, A.K. Baert, A. Vervaeta, IEICE Trans. Commun., INTELEC'03, E87–B (12) (2004) 3478–3484.

[3] B. Hirschorn, M. E. Orazem, B. Tribollet, V. Vivier, I. Frateur, M. Musiani, Electrochim. Acta 55 (2010) 6218–6227.

[4] Shih, T.-C. Lo, Electrochemical impedance spectroscopy for battery research and development, Tech. rep., Solartron Instruments (1996) .

[5] Troltzsch, O. Kanoun, H.-R. Trankler, , Electrochimica Acta 51 (89) (2006) 1664 – 1672

[6] E. Karden, S. Buller, R. W. Doncker, Journal of Power Sources, 85(1), (2000)72-78

[7] W. Lai, F. Ciucci, J. Electrochem. Soc., 158(2) (2011) A115–A121.

[8]   J. Song, M.Z. Bazant, J. Electrochem. Soc., 160(1) (2013) A15–A24.

[9] B.A. Baukamp, Electrochim. Acta, 169(1-4) (2004) 65–73.

[10] M.D. Levi and D., Electrochim. Acta, 45(1-2) (1999) 167–185.

[11] R.E.F. Einerhand, W. Visscher, J. Electrochem. Soc., 138(1) (1991) 7–17.

[12] J.P. Meyers, M. Doyle, R. M. Darling, and J. Newman, J. Electrochem. Soc., 147(8) (2000) 2930–2940.

[13] D.R. Franceschetti, J.R. Macdonald, and R.P. Buck, J. Electrochem. Soc., 138(1991) 1368-1371.

[14] J. Xie, N. Imanishi, T. Zhang, A. Hirano, Y. Takeda, and O. Yamamoto, Mater. Chem. Phys., 120(2-3) (2010) 421–425.

[15] J. Bisquert, A. Compte, J. Electroanalytical Chemistry, 499 (2001) 112-120.

[16] International Standard IEC 61960:2003, Secondary cells and batteries containing alkaline or other non-acid electrolytes. Edition 2.0, 2011-06.